Fixation of transparent bone pins with photocuring biocomposites

Fixation of transparent bone pins with photocuring biocomposites

Gautama Wicaksono[1], Felicia Toni[1], Leonard Wei Feng Tok[1], Jeanette Jun Ting Thng[1], Ivan Šolić[1], Manisha Singh[1], Ivan Djordjevic[1], Francesco Baino[2], Terry W. J. Steele*[1]

[1]School of Materials Science and Engineering (MSE), Nanyang Technological University (NTU), Singapore 639798.

[2] Institute of Materials Physics and Engineering, Department of Applied Science and Technology, Politecnico di Torino, Torino, Italy.

*Corresponding author: Terry W. J. Steele (e-mail: wjsteele@ntu.edu.sg)

ABSTRACT

Bone fractures are in need of rapid fixation methods, but current strategies are limited to metal pins and screws, which necessitate secondary surgeries upon removal. New techniques are sought to avoid surgical revisions, while maintaining or improving fixation speed. Herein, a method of bone fixation is proposed with transparent biopolymers anchored in place via light-activated, biocomposites based on expanding CaproGlu bioadhesives. The transparent biopolymers serve as a UV light guide for the activation of CaproGlu biocomposites that results in evolution of molecular nitrogen (from diazirine photolysis), simultaneously expanding the covalently crosslinked matrix. Osseointegration additives of hydroxyapatite or Bioglass 45S5 yield a biocomposite matrix with increased stiffness and pull-out strength. The structure-property relationships of UV joules dose, pin diameter, and biocomposite additives are assessed with respect to apparent viscosity, shear modulus, spatiotemporal pin curing, and lap-shear adhesion. Finally, a model system is proposed based on *ex vivo* investigation with bone tissue for the exploration and optimization of UV-active transparent biopolymer fixation.

KEY WORDS: *Bone implant fixation, polymer bioadhesive, bone biocomposite, hydroxyapatite, Bioglass.*

1. INTRODUCTION

Bone fractures are rising globally with a projected 7.5 million clinical cases by 2025 in USA and Europe, in part due to an ageing population and active lifestyles. Despite the advances in orthopaedic surgery, the rate of surgical revision and non-union fracture is alarmingly high: 10 to 50% of cases end up with failures characterized by revision surgery or non-union fracture.[1] One of the major reasons for unsuccessful bone tissue repair is suppression of blood supply to the tissue that in most cases results in non-union of the bone due to osteonecrosis, bone resorption and ischemia.[1] Biomaterials design for bone regeneration requires biomimetic approach from nano- to micro-scale. Properties of composite biomaterials like biocompatibility, degradation rate and the type/characteristics of bioactive inclusions embedded in the matrix have to be tailored to allow osseoconductivity in initial stage of healing.[2] Bone remodelling (i.e. healing) is a multi-phase process where biomechanical properties undergo dynamic change correlated to bone mineral density[3-5] as Young's modulus for human granulation tissue is ~0.5 MPa and rises up to 20 GPa for mature bone.[6] The variation of callus mechanical moduli through the multi-phase healing process can be in the range of 20-6000 MPa.[7] In case of implant-assisted fracture repair, the callus formation begins at the implant surface; the tissue formation is highly responsive to interfacial / mechanical properties of the implant and the process is known as contact osteogenesis.[8] Due to complexity of bone tissue, the development of biomaterials that would mimic bone biomechanics and structure to facilitate fracture healing still presents an unmet clinical need.[9]

Bone fixation screws and pins have been employed in clinical practice for decades. Apart from standard metallic implants,[10] bone fixation is also performed with biodegradable plates and screws that offer less invasive approaches.[11-12] Recently reported clinical trials indicate that bioresorbable polymer (polycaprolactone, PCL; poly(lactic acid), PLA) and permanent implants (metallic) are equally safe and effective for non-load-bearing bone reconstruction.[13] Resorbable implants eliminate the need for secondary surgery which is required for metallic

implants after tissue healing is completed. The bone microenvironment repair relies on sensitive bone / implant interface[14] that is disrupted by compression (force-mediated) fixation that causes peri-implant bone damage up to 0.9 mm in radial direction from the implant.[15] This issue compromises the primary implant stability and should be addressed by non-invasive, biodegradable fixation formulations that combine principles of surgical adhesion and tissue engineering.

Over the recent years we have developed a diazirine-grafted polycaprolactone polyol (named CaproGlu) hydrophobic, liquid bioadhesive that can be mixed with bone mineral hydroxyapatite to yield viscous liquid biocomposite (**Scheme 1A,B**).[16-17] The CaproGlu platform is based on polycaprolactone triol or tetrol (PCLT) grafted with trifluoromethylphenyl diazirine as a surgical adhesive.[18] UV activation of diazirine generates carbene that rapidly crosslinks with release of molecular nitrogen that causes a >200% volumetric expansion and pressures that could exceed 200 kPa (**Scheme 1C**).[19] Carbene covalently inserts non-specifically causing both internal and interfacial crosslinking that immobilizes bone implants (**Scheme 1D**).[17] Due to known biodegradation and biocompatibility of polycaprolactone biomaterials, CaproGlu-based biocomposite bone fixation formulation presents a new strategy for fixation of transparent bone pins crosslinked with low energy UV light. To the best of the authors' knowledge, there has been no prior research on utilizing photoactive, polycaprolactone-based biocomposite that mediates non-invasive fixation of light-activated bone pins.

In this paper for the first time, we describe the bone fixation with UV-active bone biocomposite based on bioactive particles, namely hydroxyapatite (both micro- and nano-particles) and glass microparticles. CaproGlu biocomposite is activated on-demand via a novel fibre-optic pin (polymethyl methacrylate; PMMA) platform (**Scheme 1C,D**). Transparent PMMA is used only as a model that simulates bone fixation by transparent,

commercially available polylactide pins (e.g. Inion CPS^{TM}).[20] Described bone biocomposite integrates tissue engineering approach with bone implant (pin) fixation where the biocomposite serves as a temporary support that evenly transfers stress from the healing tissue to the immobilized pin. The design of fibre-optic orthopaedic implant is directed by the following key requirements: (i) Biocomposite liquid conforms to the drilled gap, where activation causes volume expansion that solidifies and fills complex voids and geometries; (ii) Biocomposite is produced from biodegradable materials that induce osseointegration; (iii) Non-exothermic *in situ* crosslinking by exposure to non-invasive, low energy UV light with adhesion properties that allow flexibility towards specific bone reconstructive surgery; and (iv) Transparent fibre-optic pin made from PMMA allowing delivery of UV light that crosslinks CaproGlu component of biocomposite.

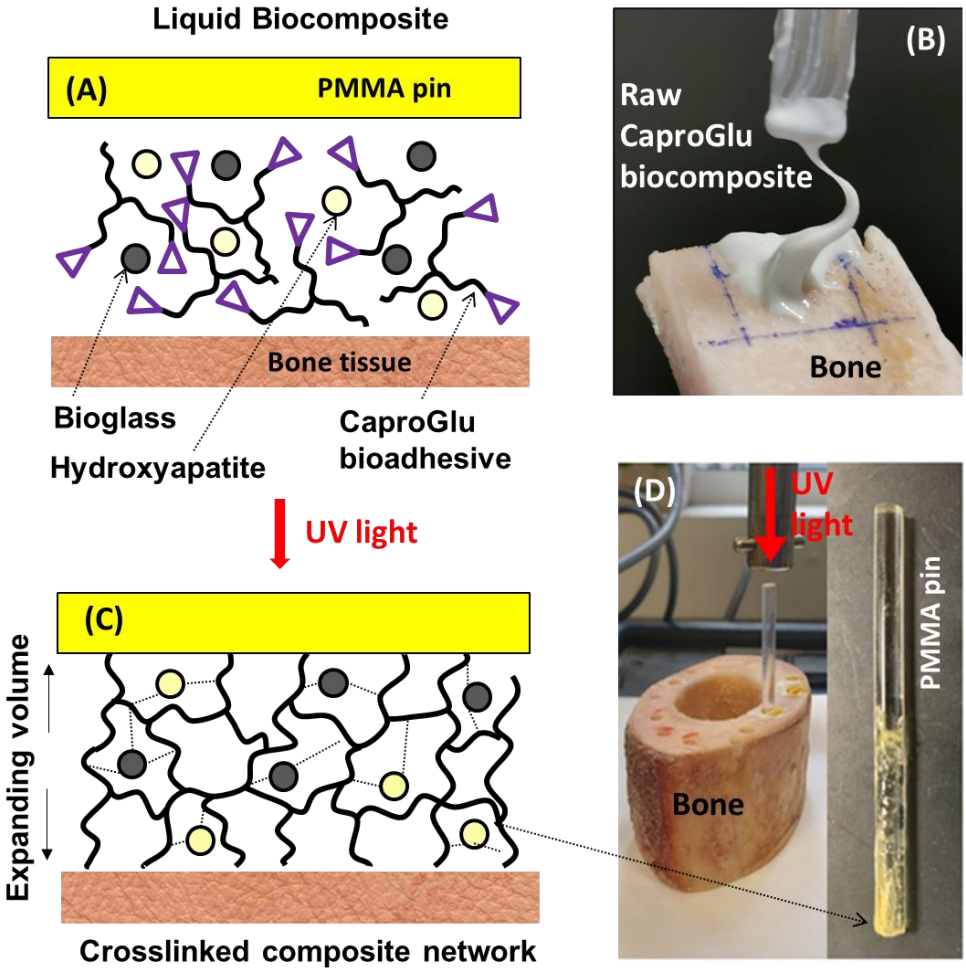

Scheme 1. Demonstration of light activation of transparent bone pins with the aid of CaproGlu biocomposite formulation. (**A**) Composite is produced by mixing diazirine-grafted polycaprolactone (CaproGlu; branched polyol with diazirine end-groups, symbolically presented as triangle shapes) with solid additives: Bioglass (45S5) and hydroxyapatite. (**B**) Representative paste-like biocomposite formulation prior to UV activation. (**C**) UV light (365 nm) transmitted through light-transparent PMMA pin activates diazirine groups and turn them into carbene for subsequent crosslinking of biocomposite at PMMA-bone interface; diazirine photolytic degradation produces molecular nitrogen bubbles that expand biocomposite and cause locking pressure for pin fixation. (**D**) *Ex-vivo* experimental setup to investigate light activation of transparent bone pins with the aid of expendable, UV-active biocomposite for mechanical locking at the bone / pin interface.

It is hypothesized that the thickness of bone-implant (pin) interface should be kept below 0.2 mm in order to ensure sufficient light transmission and UVA energy distribution and to generate sufficient interfacial crosslinking for compressive stresses that are sustained through the biocomposite matrix. The results herein present the preliminary investigations of the model system towards developing of new methods of bone fixation with non-metallic implants.

2. MATERIALS AND METHODS

2.1 Synthesis of CaproGlu bioadhesive and biocomposite preparation methodology

The detailed synthesis procedure of CaproGlu has been described in a previous publication.[16] In brief, polycaprolactone triol (CAPA 3031, 300 Da, Perstorp, Sweden) and diazirine-bromide (TCI, Japan) are mixed in PCLT/diazirine molar ratio of 1/1 to yield 50% diazirine conjugation. Reactants are dissolved in dioxane and allowed to react in the presence of silver oxide (Ag_2O) and molecular sieve for 72 h at room temperature under nitrogen atmosphere.

Filtered product is precipitated in deionized water and centrifuged; the water-dioxane supernatant is discarded and the PCLT-D conjugate product (viscous pale-yellow transparent liquid) is further washed 3 times with water and centrifuged. PCLT-D formulations are lyophilized for 24 h and characterized with ^{1}H NMR to calculate the conjugation (grafting) percentage (Bruker Avance; 400 MHz). Refractive index (RI) of purified CaproGlu is measured by Mettler Toledo portable refractometer 30GS at room temperature, and RI estimation of CaproGlu bioadhesive composites are performed using Lorentz-Lorenz equation for rule of mixtures.[21] CaproGlu bioadhesive composites are prepared by directly mixing the additive powder into the liquid CaproGlu formulation. Hydroxyapatite nanopowder (hereafter referred as HNP), <200 nm particle size are purchased from Sigma Aldrich. Hydroxyapatite coarse powder (hereafter referred as HMP), ultrapure grade (10 ± 2.0 μm particle size) were purchased from Sigma Aldrich. Bioglass 45S5 powder, <32 nm particle size (hereafter referred as BG), is synthesized by melt-quenching process followed by milling and sieving, as previously described.[22]

2.2 Photorheometry measurements

Rheometry measurements are conducted with Anton Paar Physica MCR 102 rheometer fitted with UV transparent glass plate. The applied UV intensity (365 nm) is calibrated to 100 mW cm^{-2} with an IL 1400 Radiometer through handheld UV LEDs or by Thorlabs SOLIS-365C High Power LED. Rheology tests are performed using parallel plate geometry with probe diameter 10 mm, on 0.1, 0.2 and 0.4 mm measuring gaps. Apparent viscosity is evaluated via rotational rheology with shear rate 10 s^{-1} for 60 seconds. The storage modulus (G') and loss modulus (G") are evaluated during dynamic oscillatory rheology with amplitude of 1% and frequency of 10 Hz for 160 seconds; UV irradiation is performed between t = 30 s and t = 130 s to achieve total UV dose of 10 J. Amplitude sweep of 1-1000% shear strain are performed onto the cured sample to evaluate yield stress and strain.

2.3 PMMA Optical Fiber and surface area evaluation

Optical fiber-grade PMMA rods of diameters 1 mm, 1.5 mm, 2 mm, and 3 mm were purchased from Edmund Optics Pte Ltd. The fibres are cut into 3 cm, 5 cm, or 7 cm lengths and their ends are polished using 120-grit sandpaper. Cured biocomposites on the optical fibers are taken for image analysis using ImageJ software. The images are split into RGB channels and thresholded to identify and count the ratio of pixels representing yellow-cured biocomposite against the total area. For the purpose of analysis, the cured area is split into 10 identical lengths along the direction of UV curing and the cured pixel ratio is calculated per section. The resulting % cured versus UV curing distance is fitted according Gauss probability distribution.

2.4 Shear adhesion test on ex vivo bovine femur bones

Bovine femur cortical bone samples are prepared at length of ~4 cm. Holes are drilled through the outer cortical bone with diameter of 3.4 mm; only 3 mm diameter optical fibers are tested, and the extra 0.4 mm allows ~0.2 mm thickness of biocomposite coating. Approximately 15 mg of adhesive is applied at 2.5 cm of the fiber length then inserted into drilled hole, and any excess adhesive outside the bone is removed. UV is applied at intensity 100 mW cm^{-2} for 5 minutes (30 J) through the fibre optic; excess dose is required to compensate for irregular curing efficiencies. Load is applied to the photocured PMMA pin in the axial direction, and the shear stress calculated with respect to surface area and 0.2 mm coating thickness with the aid of a modified tensile tester (Chatillon Force Measurement Products, USA) at the strain rate of 3 mm min^{-1} with 50 N capacity force cell (±0.25% resolution).

2.5 SEM/EDX analysis

CaproGlu is manually mixed with BG, HNP and HMP particles (10% w/w; solid/CaproGlu) and applied in thin layer (~50 mg) between PET sheets (sandwich structure) and cured with 10 J of UV. PETs are separated with cured CaproGlu composite on both sheets. Composite + PET is cut in 2 x 2 mm squares for SEM/EDX analysis with JEOL 5500LV electron microscope. Samples are subjected to platinum coating (90 s, chamber pressure <5 Pa at 20 mA). Images are obtained by JSM 5510 SEM at an acceleration voltage of 5–20 kV and a working distance of 15 mm. The composition of the composites is analysed by EDX using an Oxford Inca 200 EDX detector under low Vacuum and a measuring time of 300 s. Pore size distribution analysis is performed with ImageJ software by measuring the pore sizes recorded over the 7.5×10^{-3} cm^2 area. The SEM images are thresholded to outline the porous morphology and the resulting pore sizes are measured using the built-in particle analysis function.

2.6 Data analysis

All data processing, plotting and curve fitting are performed using OriginPro 2020 software. SEM Image analysis are performed using Fiji ImageJ 1.52. All biocomposite characterizations are performed in triplicate. One-way ANOVA statistical analysis is performed by Tukey's comparison and $P < 0.05$ was set as significant in all the tests.

3. RESULTS AND DISCUSSION

Nine biocomposite formulations (3 additives at 3 concentrations each) are evaluated for light activated fixation of transparent plastic implants. Several inorganic additives are available for inducing osseointegration, however we have limited the structure property relationship parameters to two different types of inorganic particles: hydroxyapatite and silica-based bioactive glass[23-25] (BG; 45S5 composition). In order to demonstrate the relationship between

mechanical properties and the size of inorganic solid phase, we report the investigation of particles in following sizes: hydroxyapatite nanoparticles and microparticles (HNP < 200 nm and HMP = 10 ± 2.0 μm, respectively) and bioactive glass (BG < 32 μm). Additive loading is hypothesized to improve the adhesive stiffness and shear adhesion strength, so each additive formulation is evaluated from 5 – 20% w/w loading. Below 5% observed no additional increase in shear modulus (vs. neat CaproGlu) and above 20% yield viscous pastes with viscosity above 10 Pa.s (**Fig. 1**). All biocomposites are evaluated by real-time photorheometry, in a multi-step protocol that yields a robust analysis of uncured liquid, joule-dependent viscoelasticity, gelation time, and strain-dependent shear modulus. The latter correlates to lap shear adhesion assuming cohesive failure. Each photorheometry experiment is done in triplicate. Three thickness profiles (0.1, 0.2, and 0.4 mm) evaluate effects of UV light attenuation through the biocomposite for total of (9 biocomposites x 3 thickness profiles x triplicates) 81 independent rheometer evaluations. Four diameters of UV transparent polymethacrylate (PMMA) are evaluated as light-transparent pins. Optical fiber-grade poly(methyl methacrylate) PMMA is required for sufficient UV transparency (hobby grades were UV opaque, data not shown). PMMA serves as a model bone pin material, as it is UV transparent, readily available, and having an elastic modulus slightly softer than cortical bone at 3 GPa.[26 27] In order to assess the lap shear adhesion at the bone implant interface, fresh *ex vivo* bovine femur bones are drilled at 3.4 mm diameter (pin diameter + 0.4 mm) and excess biocomposite is applied into a bone pin mimic, inserted into the hole. As the adhesive composite requires UV activation, the optical fiber-grade PMMA serves as the model transparent pin material.

3.1 Real-time photorheometry of composites

Biocomposites of liquid CaproGlu and three inorganic additives are prepared in three weight ratios. A multistep photorheometry protocol evaluates the biocomposites at all stages of the

curing from liquid, UV-induced gelation, to determining the strain-dependent modulus and maximum shear strain (prior to *ex vivo* experiment) with the following framework; i) parallel plate rotational shear (η_{app} UV off, 60 s), ii) oscillatory (G"/G' for 30 s UV off + 100 s UV on + 30 s UV off), iii) followed by an amplitude sweep (G"/G' from 1 – 1000%, UV off). The photorheometry setup is shown in **Fig. 1A**, with UV source below the biocomposite sample placed on a quartz surface. **Fig. 1B** shows pictures of the various composites tested: pure CaproGlu is translucent while CaproGlu mixed with BG, HNP, and HMP additives are opaque from particle light scattering. **Fig. 1C** shows the apparent viscosity as function of additive concentration, with values listed in **Table 1**.

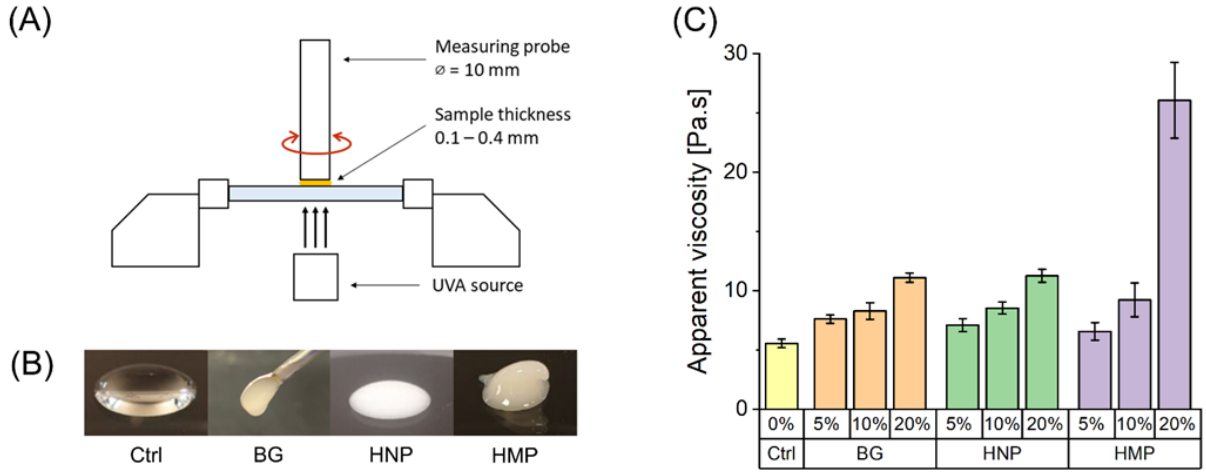

Figure 1. Photorheometry experimental setup: (**A**) Schematics presentation of rheometer fitted with light-transparent base with outlined dimension parameters. (**B**) Close-up pictures, from left to right: pure CaproGlu, CaproGlu + 20% BG, CaproGlu + 20% HNP, CaproGlu + 20% HMP. (**C**) Summary of viscosity values measured for biocomposites as a function of additive concentration in comparison to pure CaproGlu (control; 0%).

Table 1. Apparent viscosity (Pa.s) of composites: shear ^{rate} 10 s^{-1}; base-probe thickness 0.2 mm.

Additive concentration	Bioglass 45S5 (BG)	Hydroxyapatite nanopowder (HNP)	Hydroxyapatite coarse powder (HMP)
0% (control)	5.55 ± 0.37		

5%	7.60 ± 0.36	7.10 ± 0.54	6.56 ± 0.75
10%	8.29 ± 0.70	8.54 ± 0.51	9.22 ± 1.42
20%	11.1 ± 0.40	11.3 ± 0.54	26.1 ± 3.21

CaproGlu by itself (no additives) has average viscosity of 5 Pa.s. Inclusion of both BG and HNP additives up to 10% still results in viscosity lower than 10 Pa.s, and subsequent addition of solid particles increase the viscosity significantly. In particular, addition of 20% HMP displays considerable increases, likely surpassing the contact percolation threshold. Most of the uncured formulations display aspects of a Bingham plastic and are able to coat surfaces with thickness greater than 0.2 mm under the force of gravity.

Photorheometry is performed using 365 nm wavelength (defined here as UV light) at intensity of 100 $mW.cm^{-2}$ for 100 seconds, for a total dose of 10 $J.cm^{-2}$. Before UV curing, the sample is pre-sheared for 30 seconds under oscillatory rheometry, which disrupts any structures, placing the biocomposite in viscous liquid state where G" > G'. During UV exposure, CaproGlu crosslinks, evidenced by an increase in G' (storage modulus). The sample turns from viscous liquid to viscoelastic solid, represented by gelation point G' = G" (see **Fig. 2A**): an irreversible transition from liquid to elastomeric material consistency. After curing, the biocomposites are crosslinked and G' >> G". **Fig. 2A** shows a representative plot of G'' and G' versus curing time, comparing the properties of pure CaproGlu vs CaproGlu with 20% BG additive, at 0.1 mm thickness. **Fig. 2B** displays a comparison of all three additives at 20% loading, 0.2 mm thickness. An increase of G' values with BG microparticles after curing as a function of loading is presented in **Fig. 2C** and a plot of G' vs. thickness for BG, HNP and HMP is shown in **Fig. 2D**. **Table 2** lists complete values of G' after 10 J of UV curing. In addition, the process of crosslinking CaproGlu generates the maximum force of expansion which can be detected by the rheometer probe (**Table S1**). The values are

dependent on the base-probe distance and the maximum recorded force is 52 ± 6 kPa for 0.1 mm distance. The expansion force drops for an order of magnitude with increase of distance to 0.4 mm (**Table S1**). Even at the maximum value, the expansion force caused by CaproGlu crosslinking reaction is significantly lower than rupture stress measured for adult cranial human bone (100 MPa order of magnitude).[28]

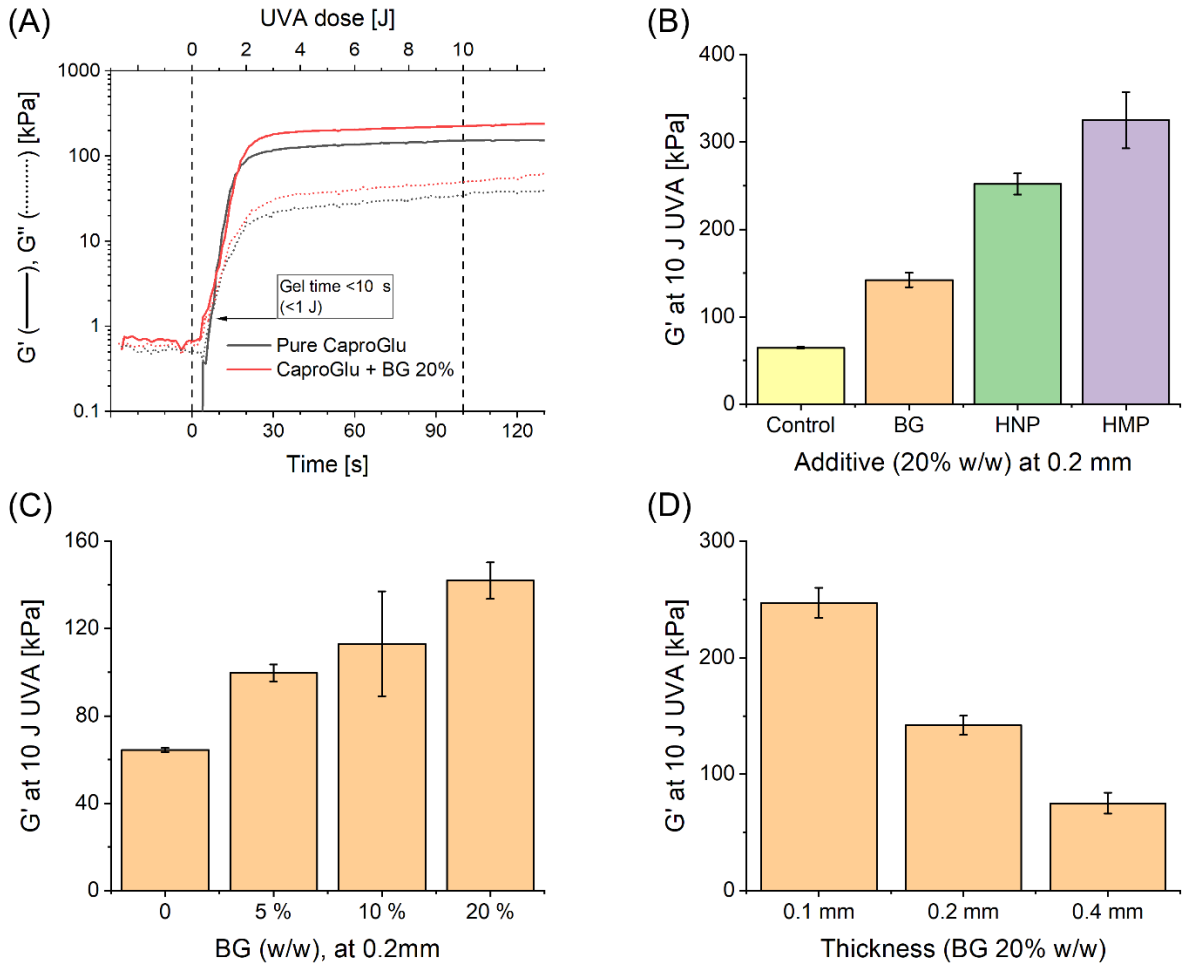

Figure 2. Photorheological properties of CaproGlu biocomposite formulations: **(A)** Plot of biocomposite photocuring showing the evolution of G' and G'' versus UV curing time, representative for pure CaproGlu vs Caproglu + 20% BG. **(B)** Comparison of G' after curing as function of additive type, representative for 20% (w/w) loading and 0.2 mm probe-base gap. **(C)** Comparison of G' after curing as function of additive loading, representative for BG and 0.2 mm thickness. **(D)** Comparison of G' after curing as a function of base-probe thickness, representative for BG at 20% (w/w) loading.

Table 2. Values of G' (storage modulus; kPa) after photocuring at total dose of 10 J.cm^{-2}.

Measurement thickness	Additive concentration (w/w)	Bioglass 45S5 (BG)	Hydroxyapatite nanopowder (HNP)	Hydroxyapatite coarse powder (HMP)
0.1 mm	0 %	155 ± 1.75		
	5 %	171 ± 35.0	172 ± 1.95	138 ± 24.9
	10 %	241 ± 35.9	191 ± 8.0	176 ± 27.6
	20 %	247 ± 12.9	250 ± 17.1	467 ± 22.1
0.2 mm	0 %	64.4 ± 0.93		
	5 %	99.6 ± 3.89	167 ± 14.6	66.3 ± 32.5
	10 %	113 ± 24	199 ± 12.6	112 ± 13.8
	20 %	142 ± 8.29	252 ± 12.2	325 ± 32
0.4 mm	0 %	49.5 ± 3.65		
	5 %	31.4 ± 1.58	54.1 ± 0.22	48.6 ± 6.67
	10 %	74.6 ± 3.56	61.2 ± 4.51	37.6 ± 2.45
	20 %	75.0 ± 8.89	67.3 ± 5.26	16.5 ± 5.02

Note that the HMP microparticles appear to have the highest light attenuation as judged by G' from 0.1 to 0.4 thickness. The rheometer probe evaluates the biocomposite surface with the least amount of light exposure. Taken together, the results suggest that thickness should be kept at 0.2 mm or smaller in order to limit gradients. Gelation point is reached within first 10 seconds of UV curing for sample thickness of 0.1 mm, up to 34 s for 0.2 mm, and 82 s for 0.4 mm (*Supplementary information:* **Fig. S1-S3)**. It is shown that osseointegration additives can

improve modulus and yield stress of CaproGlu without compromising gelation time/ gelation dose, therefore granting user control on the application of the adhesive.

Performing amplitude sweep on the UV-cured composites allows to plot a dynamic stress vs strain plot as shown in **Fig. 3A**, representative for pure CaproGlu vs CaproGlu with 20% BG additive, at 20% loading. **Fig. 3B** displays the comparison for additives at 20% loading, 0.2 mm thickness. Addition of BG up to 20% by weight greatly increases the yield stress, from 16 kPa to 58 kPa, while addition of HMP increases it up to 95 kPa. Additives loading improves stress at break, representative for BG at 0.2 mm thickness (**Fig. 3C**). The stress at yield point (break) decreases with sample thickness, as shown in **Fig. 3D** for all additives used in experiments. The complete values of stress at break are listed in **Table 3**. This points to evidence of decreasing the effectiveness of UV curing with increasing thickness.

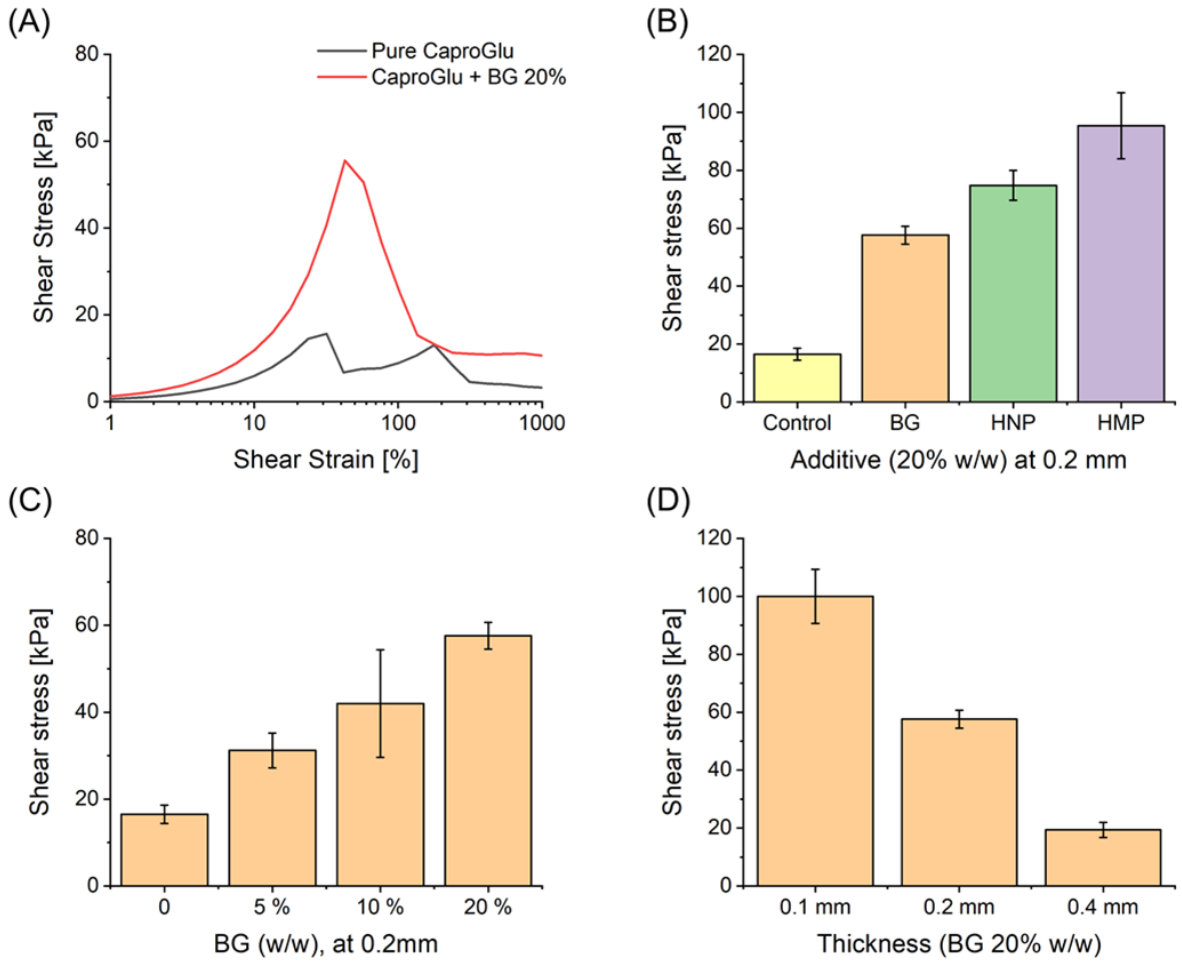

Figure 3. Rheological amplitude sweep profile of CaproGlu biocomposites: (**A**) Plot of dynamic stress vs strain of photocured biocomposite, representative for pure CaproGlu (control) vs Caproglu + 20% BG. (**B**) Comparison of stress at break as function of additive type, representative for 20% (w/w) loading and 0.2 mm thickness. (**C**) Comparison of stress at break as function of additive loading, representative for BG and 0.2 mm probe-base thickness. (**D**) Comparison of stress at break as function of thickness, representative for BG at 20% (w/w) loading.

Table 3. Shear stress (kPa) of photocured composites at yield point.

Measurement thickness	Additive concentration (w/w)	Bioglass 45S5 (BG)	Hydroxyapatite nanopowder (HNP)	Hydroxyapatite coarse powder (HMP)
0.1 mm	0 %	36.4 ± 0.33		
	5 %	56.9 ± 6.97	112 ± 2.60	71.7 ± 16.6
	10 %	78.3 ± 8.65	113 ± 4.79	84.4 ± 13.1
	20 %	100 ± 9.38	127 ± 9.51	155 ± 2.93
0.2 mm	0 %	16.5 ± 2.11		
	5 %	31.2 ± 4.02	88.7 ± 3.79	40.7 ± 20.0
	10 %	42.0 ± 12.4	85.6 ± 5.12	56.4 ± 21.5
	20 %	57.6 ± 3.1	74.8 ± 5.14	95.4 ± 11.4
0.4 mm	0 %	12.1 ± 1.52		
	5 %	9.10 ± 0.75	20.5 ± 0.66	18.8 ± 2.18
	10 %	31.3 ± 0.56	21.8 ± 2.02	12.2 ± 1.65
	20 %	19.4 ± 2.62	21.8 ± 1.71	1.78 ± 0.75

3.2 Light transmission properties of PMMA optical fiber

Optical fiber-grade PMMA of different diameters 1 mm, 1.5 mm, 2 mm, and 3 mm are cut into different lengths 3 cm, 5 cm, and 7 cm. The UV LED is fitted to a custom 3D-printed adapter to direct the light onto the 3mm diameter PMMA pin. Axial and lateral intensity measurements are performed to assess pin transparency (intensity loss) and length dependent attenuation. **Fig. 4A** shows the schematics of intensity measurement setup; for measurement

on axial direction, the PMMA optical fiber (pin) is placed directly between the UV torch and the radiometer sensor. The distance from UV source to sensor equals to the optical fiber length. For lateral direction, spectrometer is placed on the side of the PMMA optical fiber. The result of this axial intensity measurement is plotted as a function of optical fiber length and diameter (**Fig. 4B**). The control values used are intensity reading through air but at different distance, and the highest intensity achieved is 20 $mW.cm^{-2}$ at 3 cm. With increasing distance, the intensity reading reduces slightly. For lateral intensity measurement performed using a spectrometer, the results are plotted as a normalized relative light unit (**Fig. 4C**).

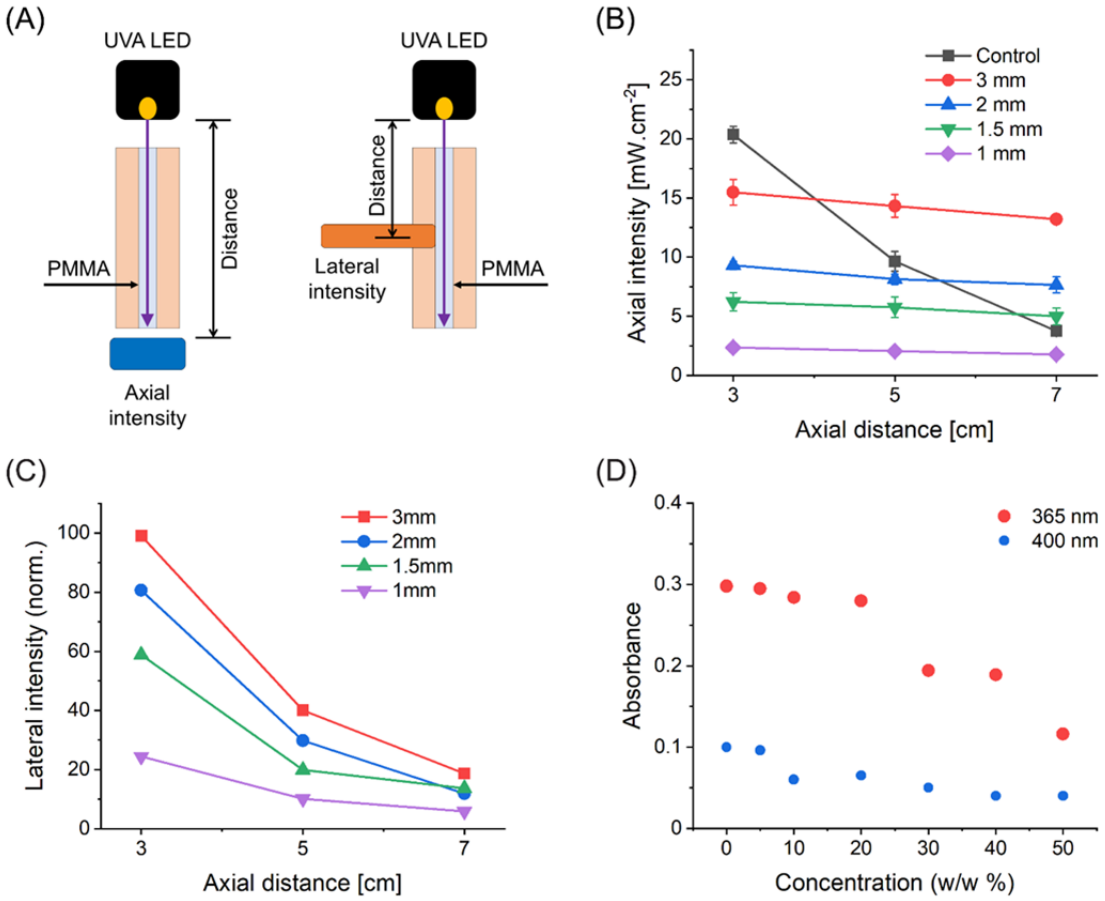

Figure 4. Optical properties of PMMA pins: (**A**) Schematic presentation of UV intensity measurement from axial and lateral directions. (**B**) Results of intensity measurement over the axial direction of PMMA optical fibers (pins) as a function of distance and optical fiber diameter; control values are measurements through air (no optical fiber). (**C**) Results of intensity measurement over the lateral direction of PMMA optical fibers as function of

distance and optical fiber diameter. (**D**) Plot of absorbance of CaproGlu + BG at representative wavelengths of 365 nm and 400 nm, showing light attenuation as function of loading concentration.

The results demonstrate that the longer the distance is, the difference between intensity readings are getting closer as dispersion starts taking effect. In both directions, the larger diameter of the optical fibers used, the more effective the light transmission becomes, and that in itself depends on the travel distance. **Fig. 4D** displays the absorbance plot of biocomposite with BG, tested at 365 nm and 400 nm, showing the light attenuation as function of loading concentration. Following the results above, for subsequent experiment results, the PMMA optical fibers with 3 mm diameter is used. Fibre length chosen is 5 cm to allow better handling of experiments.

3.3 Lap shear testing on bovine bones and refractive index of CaproGlu biocomposites

Bovine femur cortical bones are prepared with holes of 3.4 ± 0.1 mm diameter drilled into the bone. Excess biocomposites (~15 mg) are applied to 2.5 cm of the length and inserted into the bone. UV activation is performed by exposing the PMMA optical fibers with UV for 5 minutes (**Fig. 5A, left**). Subsequently, the cured adhesive is subjected to shear test by pushing the PMMA optical fiber using a tensile tester (**Fig. 5A, middle**). Once the PMMA optical fiber is removed, it is shown that the biocomposites are only partially cured down the length of the PMMA rod, with uncured region in the middle (**Fig. 5A, right**). An image analysis estimates the amount of surface curing through the clear to yellow biocomposite colour change (**Fig. 5B,C**), where the yellow tint is caused by diazoalkane formation.[29] At the air/PMMA interface, UV light is internally reflected (42^{o} critical angle, refractive index of 1.49; **Fig. 5D, i**). Internal reflection no longer occurs at the CaproGlu interface because polycaprolactone (major constituent of CaproGlu) has refractive index of 1.46, similar to

PMMA. Diffracted UV light is therefore absorbed by the biocomposite that caused crosslinking (**Fig. 5D, ii**), but the light flux decreases along the length, creating a gradient of crosslinking as function of distance from UV source. Non-uniform crosslinking caused by this effect will be addressed in future by applying more sophisticated optics than simple UVA diode used as a proof of concept in this paper (**Fig. 5A**). Regardless of recorded non-uniform light energy distribution (**Fig. 5C,D**) the reflection of UV on the opposite PMMA surface creates a second virtual light source (**Fig. 5D, iii**), which is responsible for curing from the opposite end of PMMA fiber. This explains the Gaussian distribution of biocomposite curing between real and virtual light source as seen in **Fig. 5C**.

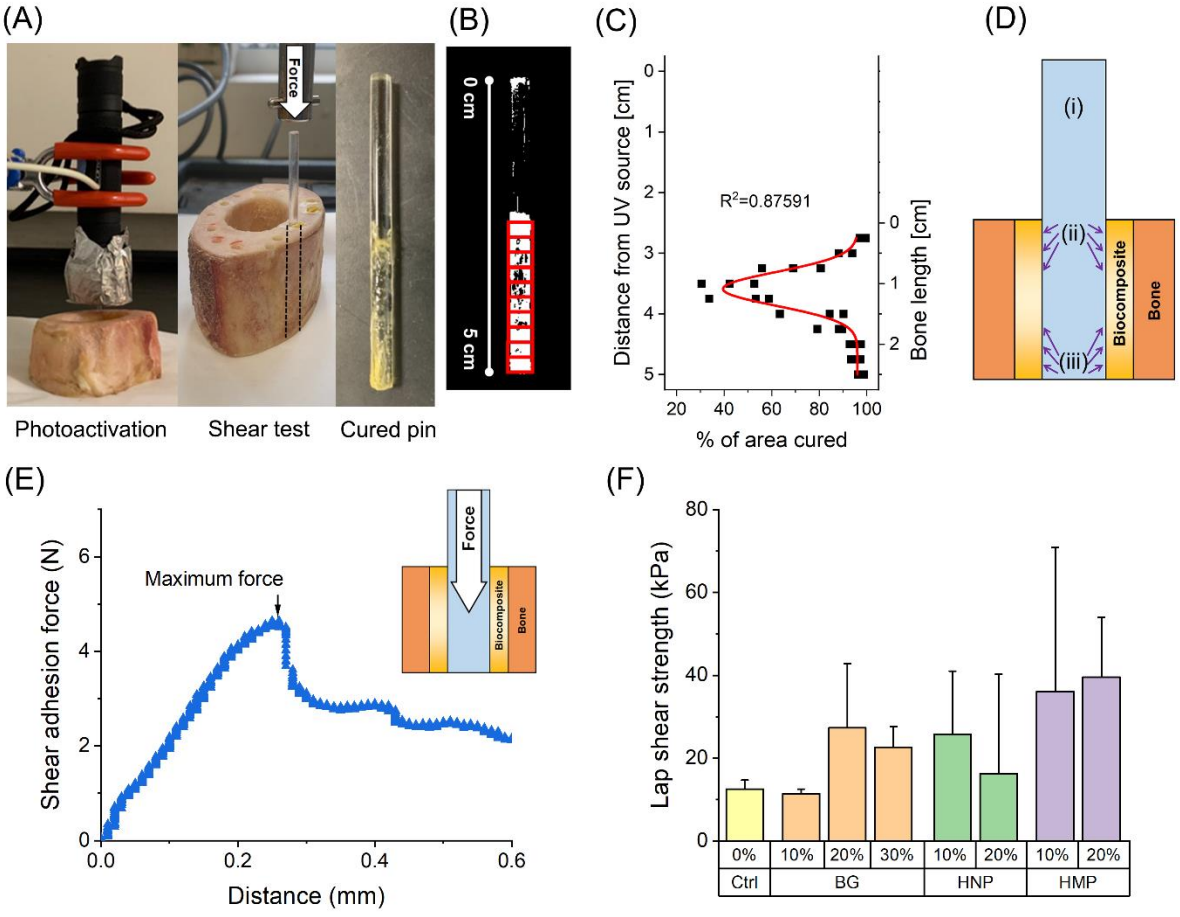

Figure 5. *Ex vivo* investigation of PMMA fixation by UV-activated CaproGlu biocomposite formulations: (**A**) *Left:* UV-curing setup of composites on PMMA optical fiber surface, inserted into holes drilled onto bovine femur bone. *Middle:* setup of shear test on bovine femur bone; the fiber optic (pin) is pushed downwards, and the shear adhesion strength is

measured (the force direction is indicated with arrow). *Right:* the composites are cured partially inside the bone. (**B**) Analysis of cured area using image editing software ImageJ by dividing cured area into 10 segments for evaluation by ratio. (**C**) Cured area ratio is fitted to Gaussian distribution with R^2 value of 0.87591. (**D**) Schematic presentation for proposed mechanism of UV curing through the PMMA fiber: (i) total internal reflection through air / PMMA medium, (ii) UV is absorbed by the biocomposite, (iii) reflection from original UV source cured the biocomposite from the opposite end of the pin. (**E**) Representative load vs distance curve of the shear test; increasing load represents the shear force experienced by cured biocomposite (*insert*: measured shear force interface). (**F**) Maximum force values from each sample is normalized against cured biocomposite area to determine lap shear strength of each biocomposite.

Figure 5E shows a representative result of this experiment on a pure CaproGlu as shear force reading at the pin-bone interface contributed by cured CaproGlu versus PMMA pin displacement, in the axial direction. As the optical fibers are sheared, load reading is increased until a maximum yield point. This value is normalized towards the cured area of adhesive, and the resulting value is defined as lap shear strength, listed in **Fig. 5F**. This ultimate shear stress value represents the adhesion (shear) strength of cured CaproGlu composite at the pin-bone interface. Curing surface area appears to be inversely dependent on the additive concentration. From 0-20% BG loading, over half the surface area is cured. There is ~10% surface curing for 30% loading and no observed curing for 40-50% loading, and therefore no lap shear adhesion results are available. As BG has high refractive index of 1.55, it is hypothesized that the biocomposite resumes total internal reflection for >30% loading,[30] explaining the lack of curing. The standard deviation remains high due to the irregular nature of the adhesive's photocuring behaviour between bone and pin surface.

This work was inspired by previous investigations of polymer waveguides that elucidated the structure activity relationships of deep tissue light delivery, transparent biopolymers, and

photochemical tissue bonding.[31] With 900 J of visible irradiation, they demonstrated a significant bonding of 2 kPa, a 5x increase over control. PMMA herein serves as the model UV-transparent biopolymer—it is available in medical grades but is not considered resorbable. The differential refractive index at the PMMA / air interface allows total internal reflection, but this immediately changes to diffraction at the PMMA/ biocomposite interface. Diffraction allows photocuring / tissue bonding of CaproGlu (up to 40 kPa), but the light flux decreases along the length of the PMMA rod, thus causing insufficient crosslinking in the center of the implant. Reflection of UV light on the opposite PMMA surface creates a virtual light source which is responsible for curing from the opposite end of PMMA pin. It is important to note that we did not observe curing with particle loading exceeding 30% BG in the biocomposite. This shows that for the current design of photocuring with transparent biopolymers, the differential refractive index between the PMMA pin (RI = 1.49) and the biocomposite (**Table 4**) was sufficient to prevent diffraction – little to no light flux prevented CaproGlu photocuring as evident from the lack of shear adhesion forces. This partial curing causes less effective biocomposite crosslinking in the middle part of the pin; as such, the current application limits to short pins where light flux can be maintained through the length of the pin.[32] Ultimately, the lower crosslinking density is likely to cause faster resorption of polycaprolactone component.[33]

Table 4. Refractive Index (RI) estimation* of CaproGlu Biocomposites.

Additive concentration (w/w)	Bioglass 45S5 (BG), RI = 1.55	Hydroxyapatite (HNP & HMP), RI = 1.64
CaproGlu	1.485 ± 0.005	
5 %	1.49	1.49
10 %	1.49	1.50
20 %	1.50	1.52
30 %	1.50	1.53

** RI estimation calculated by Lorentz-Lorenz equation for rule of mixtures.*

While shear stresses are evaluated, we speculate the broad standard deviation results from irregular photocuring and therefore no statistical significance can be gained with respect to additive comparison. Given that the hardest part of the bone is near the surface (cortical bone), bone adhesion may not be warranted within the bone marrow and optical flux may instead be minimized within the bone marrow. Part of our future work will continue to refine the optical setup to achieve precise control over light flux to reach conclusive shear adhesion test results for UV-activated transparent bone implants.

3.4 Scanning electron microscopy

Figure 6 shows representative scanning electron micrographs of UV-cured pure CaproGlu and composites with all 3 different additives (10%, w/w). The porous structure of all composites are the result of molecular nitrogen generation as byproduct of activation of diazirine from UV exposure. This is consistent with our previously reported results that demonstrate the same porous morphology of pure CaproGlu bioadhesive formulation.[17] In **Fig. 6B**, **6C**, and **6D**, the solid particles are shown embedded on the matrix as pointed on red arrows. EDX analysis confirms the composition of these particles belonging to that of BG, HNP and HMP (see **Table S2**). Image analysis shows the pore size distribution of each composite (**Fig. S4**) with measured pore sizes for CaproGlu (control), BG. HNP and HMP of: 43 ± 39 μm, 26 ± 19 μm, 41 ± 31 μm and 37 ± 26 μm, respectively, which is in line of previously reported ~ 50 μm pore size of CaproGlu[34]. It should be noted that nanoparticle load (HNP) caused significantly lower pore size in comparison to both control and microparticle-embedding composite (HMP and BG; **Fig. S4**).

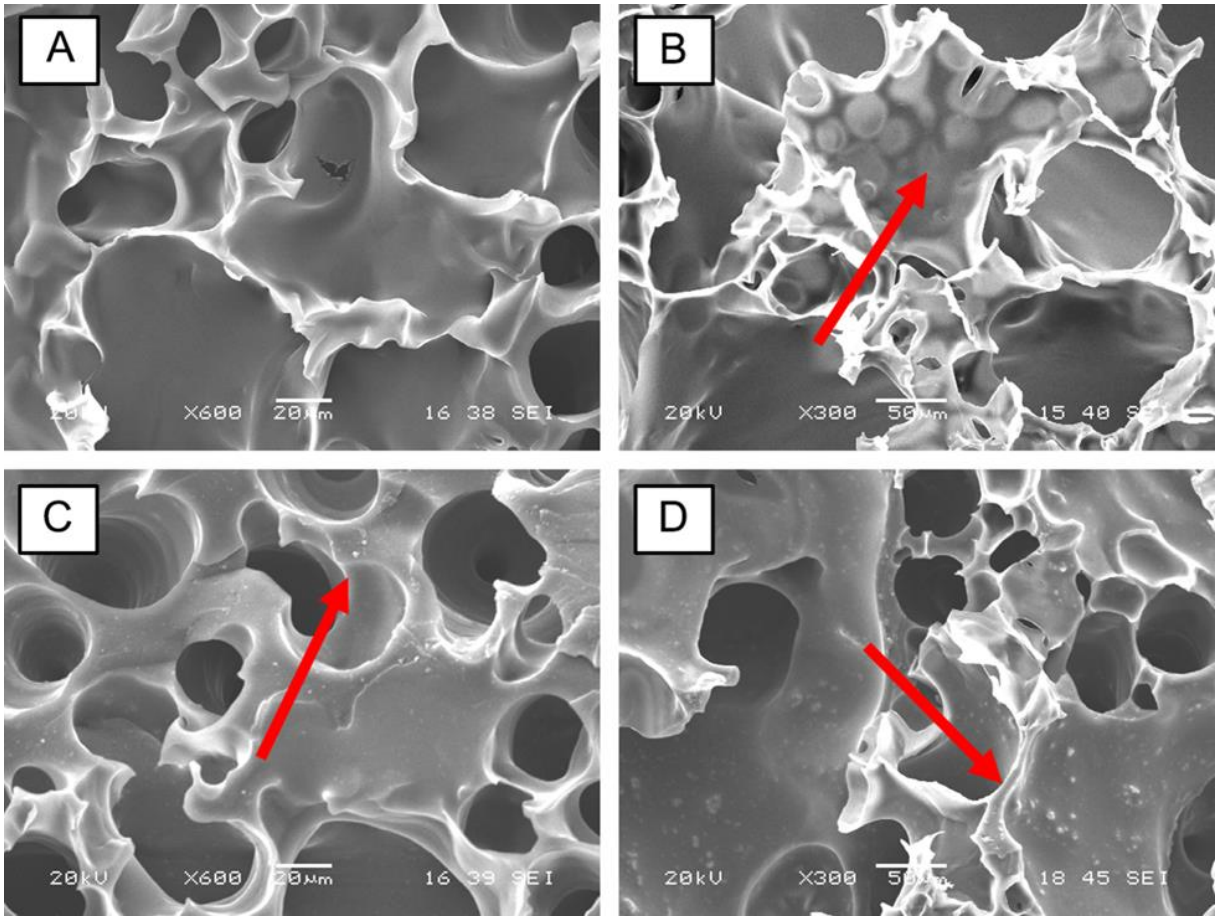

Figure 6. Morphological analysis of crosslinked CaproGlu biocomposites (UV; 10 J) by scanning electron microscopy (SEM; arrows indicate embedded mineral particles in polymer matrix): (**A**) pure CaproGlu (control). CaproGlu composites with: (**B**) Bioglass 45S5 (10%); **(C)** hydroxyapatite nanoparticles (10%); and **(D)** hydroxyapatite microparticles (10%).

CaproGlu bioadhesive is designed as a solvent-free liquid pre-polymer that allows incorporation of inorganic additives, such as hydroxyapatite and Bioglass 45S5 (**Fig. 1**). Previous evaluation of CaproGlu composites displayed adhesion strength > 800 kPa on cranium substrates.[16] Generation of molecular nitrogen as byproduct of diazirine activation allows the initially liquid-like CaproGlu adhesive to expand into porous matrix, that fills gaps between surfaces during photocuring, forming a solid porous matrix (**Fig. 6**). Herein, the bone adhesion and light-activated expansion is exploited towards fixation at the implant-bone interface.

As hypothesized, confining the thickness of bone-implant interface below 0.2 mm in conjunction to transparent cylindrical bone pin, compressive stresses have been generated through the adhesive matrix - a crosslinked biocomposite layer forms *in situ* at the implant-bone interface. Such unique behaviour is deemed less traumatic than compressive stresses formed by screws or pressure-fit pins: the Young's modulus of bone changes during healing in the range of 20 – 6,000 MPa[7], and residual compressive stresses could form because of difference in modulus. With a crosslinked biocomposite layer acting as a mediation between implant and bone, this modulus mismatch between implant and bone can be minimized, therefore minimizing risk of complications.[34-35] The expanding matrix may act as a porous scaffold towards cell migration and neovascularization during remodelling stage of bone fracture healing. SEM images (**Fig. 6**) suggests that the osseointegration additive particles of Bioglass 45S5 and hydroxyapatite are embedded onto the surface of the porous matrix, which is expected to promote further bone healing.

Additives to liquid polymers can plasticize the matrix[19, 36] while solid additives improve the modulus and adhesive strength of photocured CaproGlu (**Fig. 2; Table 2**). Inorganic additives of Bioglass 45S5 and hydroxyapatite have enough fluidity to be applied by syringe, but with sufficient viscosity to allow sub-millimetre coatings to be applied. HMP additive shows the largest viscosity increase, as its μm-particle size is an order of magnitude larger than the HNP. As a result, its composite at 20% (w/w) have significantly increased viscosity (**Fig. 1**). Loading concentration of additives generally increases dynamic modulus of photocured biocomposite. Different types of additives result in different curing profiles (**Fig. S1-S3**). Photocuring itself is dependent on the penetration of UV light through the matrix, which is limited by thickness of the adhesive applied. Future designs will continue to optimize the curing through the matrix, which is one detractor of light activated bioadhesives.

CaproGlu composite's unique material properties sets it apart from conventional implant fixation by commercial cements, such as acrylate (i.e. Cemex®, Simplex™) or ceramic (i.e. Norian®, HydroSet®) formulations.[37-39] Although the clinical use of modern acrylates dates back to 1943[40] the next generation of fixatives seeks to avoid acrylates-based polymerization due to their unresorbable nature, immunological rejection, and further injury due to mechanical mismatch with native osteo-tissues.[41] Free-radical polymerization can be activated by light-based mechanisms or two-part mixing, but the bulk of these adhesives requires free radical initiators and preservatives that leach into surrounding tissues. The exothermic reactions can heat up to 100°C[42] if no cooling is factored into the application. Modulus can only be grossly controlled, further exacerbating tissue sensitivity.[41] Bone cements have the advantage of rapid fixation, but have known risks with regards to fixation / fracture failure (through accumulation of microcracks) and toxic systemic risks (bone cement implantation syndrome) caused by initiator / monomer leachates from the shrinking acrylate resins.[43] Calcium phosphate-based cements (CPCs) were developed to overcome acrylate impediments with major advantages over acrylates, such as osteoconductivity, osteoinductivity, bio-resorbability, and interaction with bone cells. Although CPCs are of biocompatible nature, they cannot be activated on-demand, have low mechanical strength and exhibit low interfacial adhesion with hydrated tissues.[44] Thus, there is still an unmet clinical need for bone-interface fixation formulations capable for non-invasive activation without exothermic crosslinking reaction and toxic leachates: features demonstrated by CaproGlu biocomposites described in this work.

The results reported in this paper present novel CaproGlu composite platform as potential alternative to conventional bone implant fixation formulations (i.e. acrylates, CPCs). An ideal bone implant fixation formulation should have the following properties: (1) blood and bone tissue compatibility, (2) sufficient mechanical strength to stabilize fracture, (3) straight-

forward and simplified application on hard-to-reach areas, and (4) bone healing mediation.[45] The combination of UV curing and tunable viscosity by changing additive concentrations allows greater control of adhesive application where commercial bone fixation acrylates lack (i.e. spontaneous reaction, exothermic effect, toxic leachates). Gelation time is not affected by additive content, therefore the amount of UV dose can be kept to a minimum. Porous structure resulting from diazirine photolysis/nitrogen generation reduces the stiffness of the matrix, but can be beneficial in two ways: first, access is available for bone growth through the matrix, and second, the expansion of matrix allows the adhesive to fill implant/tissue gaps more efficiently. These advantages are not without drawbacks; as the effectiveness of UV curing is decreasing with thickness, care should be taken when applying adhesive to avoid incomplete curing. The resulting implant adhesion (shear) strength remains to be improved by a factor of 10 – 100x for load bearing applications, but may meet less strenuous, non-loading bearing applications. Our future work will continue to improve the adhesion strength of light activated bone implants while expanding the technology to the latest materials available for transparent waveguides.[46-48]

In vivo investigation of CaproGlu has previously demonstrated moderate immunological response[16]. CaproGlu was also assessed by OECD-regulated *in vitro* tests that demonstrated no sensitization or genotoxic effect.[17] CaproGlu is polycaprolactone-based crosslinked material that is biodegradable like its predecessors: the family of biodegradable polymers with well-defined degradation mechanism (ester hydrolysis flushed through metabolic pathways) and the range of different degradation kinetics based on crosslinking density (i.e. polymerization time, molecular weight).[33, 49-50] In our previous *in vivo* work (rabbit model) we have observed CaproGlu resorption within 1-3 weeks due to the porous nature of UVA-activated CaproGlu bioadhesive layer in close contact with blood vessels.[16] Like all biodegradable materials, the degradation kinetics of CaproGlu biocomposite is anticipated to

be dependent on several factors, including the parameters reported in this paper: concentration / size / type of solid bioactive particles as well as the crosslinking density dependent on CaproGlu molecular weight / diazirine grafting percentage / UVA energy dose. Dedicated biodegradation study is currently conducted in our laboratory and the results will be reported in future.

5. Conclusion

A unique strategy of bone fixation by UV light activation of transparent biopolymers is demonstrated through the unique CaproGlu biocomposites. CaproGlu-based biocomposites combination of rapid expansion and interfacial crosslinking provide a less traumatic method of bone implant fixation compared to metal pins or screws. When mixed with bioactive solid additives, liquid CaproGlu yields composites that have tunable mechanical properties controlled by; (i) concentration of solid particles in the composite; (ii) particle size; and (iii) joules light dose. The synthetic nature of CaproGlu, straight-forward production of composites by simple mixing, interfacial sustainability to applied mechanical load and non-invasive crosslinking strategy, opens a pathway for future bone fixation devices based on transparent biopolymers.

ASSOCIATED CONTENT

Supporting Information

Supporting information contains the extended photorheometry data (**Fig. S1-S3; Table S1**), pore size distribution measured form SEM images (**Fig. S4**) and EDX results (**Table S2**).

AUTHOR INFORMATION

Author Contributions

The manuscript was produced through contributions from all listed authors. The final version of the manuscript is approved by all listed authors.

DECLARATION OF CONFLICT OF INTEREST

T.W.J. Steele and I. Djordjevic are co-inventors of patent application: Hygroscopic, Cross-linking Coatings and Bioadhesives; PCT/SG2018/050452. Authors declare no competing interests.

FUNDING SOURCES

Ministry of Education Tier 1 Grant RG17/18 (S): Novel light activated, diazo protecting groups, Ministry of Education Tier 2 Grant (MOE2018-T2-2-114): CaproGlu, Double sided wet-tissue adhesives, NTUitive POC (Gap) Fund NGF/2018/05: Aesthetic Applications of CaproGlu Bioadhesives, and A*Star IAF PP Grant (H19/01/a0/0II9): CathoGlu Bioadhesives-preventing catheter extravasation and skin infections.

References

1. Lopes, D.; Martins-Cruz, C.; Oliveira, M. B.; Mano, J. F., Bone physiology as inspiration for tissue regenerative therapies. *Biomaterials* **2018,** *185*, 240-275.
2. Dan Wang, J. R. G., Xu Zhang, Bingkun Zhao, Dai Fei Elmer Ker, and Gregory M. Cooper, Calvarial Versus Long Bone: Implications for Tailoring Skeletal Tissue Engineering. *Tissue Engineering Part B: Reviews* **2020,** *26* (1), 46-63.
3. Christel, P.; Cerf, G.; Pilla, A., Time evolution of the mechanical properties of the callus of fresh fractures. *Annals of Biomedical Engineering* **1981,** *9* (4), 383-391.
4. Bahney, C. S.; Zondervan, R. L.; Allison, P.; Theologis, A.; Ashley, J. W.; Ahn, J.; Miclau, T.; Marcucio, R. S.; Hankenson, K. D., Cellular biology of fracture healing. *J Orthop Res* **2019,** *37* (1), 35-50.
5. Suzuki, T.; Matsuura, Y.; Yamazaki, T.; Akasaka, T.; Ozone, E.; Matsuyama, Y.; Mukai, M.; Ohara, T.; Wakita, H.; Taniguchi, S.; Ohtori, S., Biomechanics of callus in the bone healing process, determined by specimen-specific finite element analysis. *Bone* **2020,** *132*, 115212.

6. Richardson, J.; Cunningham, J.; Goodship, A.; O'connor, B.; Kenwright, J., Measuring stiffness can define healing of tibial fractures. *The Journal of bone and joint surgery. British volume* **1994,** *76* (3), 389-394.
7. Kim, H.-J.; Chang, S.-H.; Jung, H.-J., The simulation of tissue differentiation at a fracture gap using a mechano-regulation theory dealing with deviatoric strains in the presence of a composite bone plate. *Composites Part B: Engineering* **2012,** *43* (3), 978-987.
8. Shah, F. A.; Ruscsák, K.; Palmquist, A., 50 years of scanning electron microscopy of bone—a comprehensive overview of the important discoveries made and insights gained into bone material properties in health, disease, and taphonomy. *Bone Research* **2019,** *7* (1), 15.
9. Stahel, P. F.; Alfonso, N. A.; Henderson, C.; Baldini, T., Introducing the "Bone-Screw-Fastener" for improved screw fixation in orthopedic surgery: a revolutionary paradigm shift? *Patient Safety in Surgery* **2017,** *11* (1), 6.
10. Bali, R. K.; Sharma, P.; Jindal, S.; Gaba, S., To evaluate the efficacy of biodegradable plating system for fixation of maxillofacial fractures: A prospective study. *Natl J Maxillofac Surg* **2013,** *4* (2), 167-172.
11. Degala, S.; Shetty, S.; Ramya, S., Fixation of zygomatic and mandibular fractures with biodegradable plates. *Ann Maxillofac Surg* **2013,** *3* (1), 25-30.
12. Ali, A. A. A.; Kabbash, M. M.; Said, S. M. A.; Shoeib, M. A.; Osman, M. H., Use of biodegradable plates and screws in the treatment of pediatric facial bone fractures. *Egyptian Journal of Oral & Maxillofacial Surgery* **2016,** *7* (3), 86-93.
13. Seen, S.; Young, S. M.; Teo, S. J.; Lang, S. S.; Amrith, S.; Lim, T. C.; Sundar, G., Permanent Versus Bioresorbable Implants in Orbital Floor Blowout Fractures. *Ophthalmic plastic and reconstructive surgery* **2018,** *34* (6), 536-543.
14. Yi, H.; Ur Rehman, F.; Zhao, C.; Liu, B.; He, N., Recent advances in nano scaffolds for bone repair. *Bone Research* **2016,** *4* (1), 16050.
15. Steiner, J. A.; Ferguson, S. J.; van Lenthe, G. H., Screw insertion in trabecular bone causes peri-implant bone damage. *Medical engineering & physics* **2016,** *38* (4), 417-22.
16. Djordjevic, I.; Pokholenko, O.; Shah, A. H.; Wicaksono, G.; Blancafort, L.; Hanna, J. V.; Page, S. J.; Nanda, H. S.; Ong, C. B.; Chung, S. R.; Chin, A. Y. H.; McGrouther, D.; Choudhury, M. M.; Li, F.; Teo, J. S.; Lee, L. S.; Steele, T. W. J., CaproGlu: Multifunctional tissue adhesive platform. *Biomaterials* **2020,** *260*, 120215.
17. Djordjevic, I.; Wicaksono, G.; Solic, I.; Steele, T. W., In Vitro Biocompatibility of Diazirine‐Grafted Biomaterials. *Macromolecular Rapid Communications* **2020**, 2000235.
18. Steele, T. W. J.; Djordjevic, I., HYGROSCOPIC, CROSSLINKING COATINGS AND BIOADHESIVES, PCT/SG2018/050452. *PCT/SG2018/050452* **2019**.
19. Shah, A.; Pilla, K.; Gandhi, P.; Jonnalagadda, K.; Steele, T., Pulsed Laser Activation of Carbene Bioadhesive Boosts Bonding Strength. *Macromolecular Materials and Engineering.* **2019**, Accepted.
20. Gareb, B.; Roossien, C. C.; van Bakelen, N. B.; Verkerke, G. J.; Vissink, A.; Bos, R. R. M.; van Minnen, B., Comparison of the mechanical properties of biodegradable and titanium osteosynthesis systems used in oral and maxillofacial surgery. *Scientific Reports* **2020,** *10* (1), 18143.
21. Mehra, R., Application of refractive index mixing rules in binary systems of hexadecane and heptadecane withn-alkanols at different temperatures. *Journal of Chemical Sciences* **2003,** *115* (2), 147-154.
22. Baino, F.; Fiume, E., Quantifying the effect of particle size on the crystallization of 45S5 bioactive glass. *Materials Letters* **2018,** *224*, 54-58.
23. Fiume, E.; Barberi, J.; Verné, E.; Baino, F., Bioactive Glasses: From Parent 45S5 Composition to Scaffold-Assisted Tissue-Healing Therapies. *Journal of Functional Biomaterials* **2018,** *9* (1).

24. Baino, F.; Verné, E.; Fiume, E.; Peitl, O.; Zanotto, E. D.; Brandão, S. M.; Schellini, S. A., Bioactive glass and glass-ceramic orbital implants. *International Journal of Applied Ceramic Technology* **2019,** *16* (5), 1850-1863.
25. Kargozar, S.; Kermani, F.; Mollazadeh Beidokhti, S.; Hamzehlou, S.; Verné, E.; Ferraris, S.; Baino, F., Functionalization and Surface Modifications of Bioactive Glasses (BGs): Tailoring of the Biological Response Working on the Outermost Surface Layer. *Materials* **2019,** *12* (22).
26. Ali, U.; Karim, K. J. B. A.; Buang, N. A., A Review of the Properties and Applications of Poly (Methyl Methacrylate) (PMMA). *Polymer Reviews* **2015,** *55* (4), 678-705.
27. Peters, K., Polymer optical fiber sensors—a review. *Smart Materials and Structures* **2010,** *20* (1), 013002.
28. Motherway, J. A.; Verschueren, P.; Van der Perre, G.; Vander Sloten, J.; Gilchrist, M. D., The mechanical properties of cranial bone: The effect of loading rate and cranial sampling position. *Journal of Biomechanics* **2009,** *42* (13), 2129-2135.
29. Djordjevic, I.; Wicaksono, G.; Solic, I.; Steele, T. W. J., Diazoalkane decay kinetics from UVA-active protein labelling molecules: Trifluoromethyl phenyl diazirines. *Results in Chemistry* **2020,** *2*, 100066.
30. Reis, J. C. R.; Lampreia, I. M. S.; Santos, Â. F. S.; Moita, M. L. C. J.; Douhéret, G., Refractive Index of Liquid Mixtures: Theory and Experiment. *ChemPhysChem* **2010,** *11* (17), 3722-3733.
31. Nizamoglu, S.; Gather, M. C.; Humar, M.; Choi, M.; Kim, S.; Kim, K. S.; Hahn, S. K.; Scarcelli, G.; Randolph, M.; Redmond, R. W., Bioabsorbable polymer optical waveguides for deep-tissue photomedicine. *Nature communications* **2016,** *7*.
32. Turvey, T. A.; Proffit, W. P.; Phillips, C., Biodegradable fixation for craniomaxillofacial surgery: a 10-year experience involving 761 operations and 745 patients. *Int J Oral Maxillofac Surg* **2011,** *40* (3), 244-249.
33. Abrisham, M.; Noroozi, M.; Panahi-Sarmad, M.; Arjmand, M.; Goodarzi, V.; Shakeri, Y.; Golbaten-Mofrad, H.; Dehghan, P.; Seyfi Sahzabi, A.; Sadri, M.; Uzun, L., The role of polycaprolactone-triol (PCL-T) in biomedical applications: A state-of-the-art review. *European Polymer Journal* **2020,** *131*, 109701.
34. Shah, A. H.; Pokholenko, O.; Nanda, H. S.; Steele, T. W. J., Non-aqueous, tissue compliant carbene-crosslinking bioadhesives. *Materials Science and Engineering: C* **2019,** *100*, 215-225.
35. Kim, Y.-T.; Hitchcock, R. W.; Bridge, M. J.; Tresco, P. A., Chronic response of adult rat brain tissue to implants anchored to the skull. *Biomaterials* **2004,** *25* (12), 2229-2237.
36. Wicaksono, G.; Djordjevic, I.; Shah, A. H.; Steele, T. W. J., Photorheology of bioadhesive dendrimer polycaprolactone composites. *Polymer Testing* **2019,** *80*, 106099.
37. Barralet, J. E.; Duncan, C. O.; Dover, M. S.; Bassett, D. C.; Nishikawa, H.; Monaghan, A.; Gbureck, U., Cortical bone screw fixation in ionically modified apatite cements. *Journal of Biomedical Materials Research Part B: Applied Biomaterials* **2005,** *73B* (2), 238-243.
38. Cavalu, S., Acrylic Bone Cements: New Insight and Future Perspective. *Key Engineering Materials* **2017,** *745*, 39-49.
39. Lee, C. M.; Engelbrecht, C. J.; Soper, T. D.; Helmchen, F.; Seibel, E. J., Scanning fiber endoscopy with highly flexible, 1-mm catheterscopes for wide-field, full-color imaging. *Journal of biophotonics* **2010,** *3* (5-6), 385.
40. Bistolfi, A.; Ferracini, R.; Albanese, C.; Vernè, E.; Miola, M., PMMA-Based Bone Cements and the Problem of Joint Arthroplasty Infections: Status and New Perspectives. *Materials (Basel)* **2019,** *12* (23), 4002.

41. Saleh, K. J.; El Othmani, M. M.; Tzeng, T. H.; Mihalko, W. M.; Chambers, M. C.; Grupp, T. M., Acrylic bone cement in total joint arthroplasty: A review. *Journal of Orthopaedic Research* **2016,** *34* (5), 737-744.
42. Kawashita, M.; Kawamura, K.; Li, Z., PMMA-based bone cements containing magnetite particles for the hyperthermia of cancer. *Acta Biomaterialia* **2010,** *6* (8), 3187-3192.
43. Juvonen, T.; Nuutinen, J.-P.; Koistinen, A. P.; Kröger, H.; Lappalainen, R., Biomechanical evaluation of bone screw fixation with a novel bone cement. *BioMedical Engineering OnLine* **2015,** *14* (1), 74.
44. Yousefi, A.-M., A review of calcium phosphate cements and acrylic bone cements as injectable materials for bone repair and implant fixation. *Journal of Applied Biomaterials & Functional Materials* **2019,** *17* (4), 2280800019872594.
45. Sánchez-Fernández, M. J.; Hammoudeh, H.; Félix Lanao, R. P.; van Erk, M.; van Hest, J. C. M.; Leeuwenburgh, S. C. G., Bone-Adhesive Materials: Clinical Requirements, Mechanisms of Action, and Future Perspective. *Advanced Materials Interfaces* **2019,** *6* (4), 1802021.
46. Farajikhah, S.; Runge, A. F. J.; Boumelhem, B. B.; Rukhlenko, I. D.; Stefani, A.; Sayyar, S.; Innis, P. C.; Fraser, S. T.; Fleming, S.; Large, M. C. J., Thermally drawn biodegradable fibers with tailored topography for biomedical applications. *Journal of Biomedical Materials Research Part B: Applied Biomaterials* **2021,** *109* (5), 733-743.
47. Prajzler, V.; Arif, S.; Min, K.; Kim, S.; Nekvindova, P., All-polymer silk-fibroin optical planar waveguides. *Optical Materials* **2021,** *114*, 110932.
48. Rezapour Sarabi, M.; Jiang, N.; Ozturk, E.; Yetisen, A. K.; Tasoglu, S., Biomedical optical fibers. *Lab on a Chip* **2021,** *21* (4), 627-640.
49. Woodruff, M. A.; Hutmacher, D. W., The return of a forgotten polymer—Polycaprolactone in the 21st century. *Progress in polymer science* **2010,** *35* (10), 1217-1256.
50. Lam, C. X.; Savalani, M. M.; Teoh, S.-H.; Hutmacher, D. W., Dynamics of in vitro polymer degradation of polycaprolactone-based scaffolds: accelerated versus simulated physiological conditions. *Biomedical materials* **2008,** *3* (3), 034108.